PERGAMON

International Journal of Solids and Structures 40 (2003) 5923–5948

INTERNATIONAL JOURNAL OF SOLIDS and STRUCTURES

www.elsevier.com/locate/ijsolstr

Analytical solutions for tapering quadratic and cubic rat-holes in highly frictional granular solids

Ngamta Thamwattana *, James M. Hill *

School of Mathematics and Applied Statistics, University of Wollongong, Wollongong, NSW 2522, Australia

Received 14 February 2003; received in revised form 26 June 2003

Abstract

New exact analytical solutions are presented for both stress and velocity fields for a Coulomb–Mohr granular solid assuming non-dilatant double-shearing theory. The solutions determined apply to highly frictional materials for which the angle of internal friction ϕ is assumed equal to 90°. This major assumption is made primarily to facilitate exact analytical solutions, and it is discussed at length in the Introduction, both in the context of real materials which exhibit large angles of internal friction, and in the context of using the solutions derived here as the leading term in a regular perturbation solution involving powers of $1 - \sin\phi$. The analytical velocity fields so obtained are illustrated graphically by showing the direction of the principal stress as compared to the streamlines. The stress solutions are also exploited to determine the static stress distribution for a granular material contained within vertical boundaries and a horizontal base, which is assumed to have an infinitesimal central outlet through which material flows until a rat-hole of parabolic or cubic profile is obtained, and no further flow takes place. A rat-hole is a stable structure that may form in storage hoppers and stock-piles, preventing any further flow of material. Here we consider the important problems of two-dimensional parabolic rat-holes of profile $y = ax^2$, and three-dimensional cubic rat-holes of profile $z = ar^3$, which are both physically realistic in practice. Analytical solutions are presented for both two and three-dimensional rat-holes for the case of a highly frictional granular solid, which is stored at rest between vertical walls and a horizontal rigid plane, and which has an infinitesimal central outlet. These solutions are bona fide exact solutions of the governing equations for a Coulomb–Mohr granular solid, and satisfy exactly the free surface condition along the rat-hole surface, but approximate frictional conditions along the containing boundaries. The analytical solutions presented here constitute the only known solutions for any realistic rat-hole geometry, other than the classical solution which applies to a perfectly vertical cylindrical cavity.

Keywords: Granular materials; Coulomb–Mohr yield condition; Non-dilatant double-shearing theory; Highly frictional materials; Curved rat-holes; Exact parametric analytical solutions

* Corresponding authors. Tel.: +61-2-4221-3845; fax: +61-2-4221-4845.
E-mail addresses: nt59@uow.edu.au (N. Thamwattana), jhill@uow.edu.au (J.M. Hill).

0020-7683/$ - see front matter © 2003 Elsevier Ltd. All rights reserved.
doi:10.1016/S0020-7683(03)00395-0

1. Introduction

A rat-hole is a stable two-dimensional slot or channel, or three-dimensional cylindrical cavity, that may form in storage hoppers and stockpiles and prevent further material falling through the outlet. It is not a desirable phenomena for any industry because it disrupts the flow of the material. Removing a stable rat-hole from a stockpile or hopper is an additional manual procedure that costs both time and money, and which may be dangerous, since people have died from attempting to remove stable rat-holes formed in grain silos. Very little theoretical information is known about the formation of rat-holes, and whether an existing formed rat-hole is stable or unstable. These are important issues, that have yet to be properly addressed in the literature. In this paper we present exact analytical solutions for both the two and three-dimensional tapering rat-holes depicted in Figs. 1 and 2. We note that such rat-holes have not been studied previously, and our solutions constitute the only known analytical solutions for these physically realistic situations. These exact solutions for the non-dilatant double-shearing theory and the Coulomb–Mohr yield condition, are obtained by assuming that the angle of internal friction $\phi = 90°$. Physically, this assumption might not be precisely realizable, but mathematically, the solutions presented provide the limiting behavior for real materials which might be termed "highly frictional granular materials", which do indeed exist as evidenced by the data in Table 1. This assumption is discussed at length subsequently, but here we simply note that for those problems which may be solved numerically for the full range $0 \leqslant \phi \leqslant \pi/2$, such as the problem of gravity flow from a hopper (Hill and Cox, 2001b) the case $\phi = \pi/2$ is seen to behave both qualitatively and quantitatively the same as other values of ϕ such as $\phi = \pi/3$ and $\pi/6$.

Jenike (1962a,b) and Jenike and Yen (1962a,b) attempt to establish a theory of rat-hole stability, usually termed classical rat-hole theory. However, Hill and Cox (2000) re-examine this theory and show that some of the assumptions of the so-called "Jenike stable rat-hole equation" are invalid. Practising engineers believe that classical rat-hole theory does not reflect actual material behavior. One of the reasons that classical rat-hole theory is not well accepted is because a rat-hole is assumed to be a perfectly vertical cylindrical cavity with stresses within the rat-hole which are independent of height. In reality, rat-holes tend to exhibit

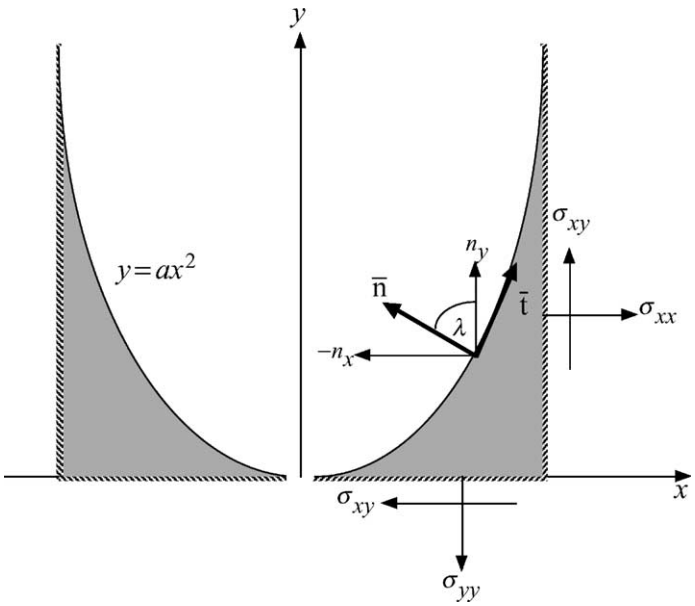

Fig. 1. Coordinates for the two-dimensional quadratic rat-hole showing stresses on the horizontal and vertical boundaries.

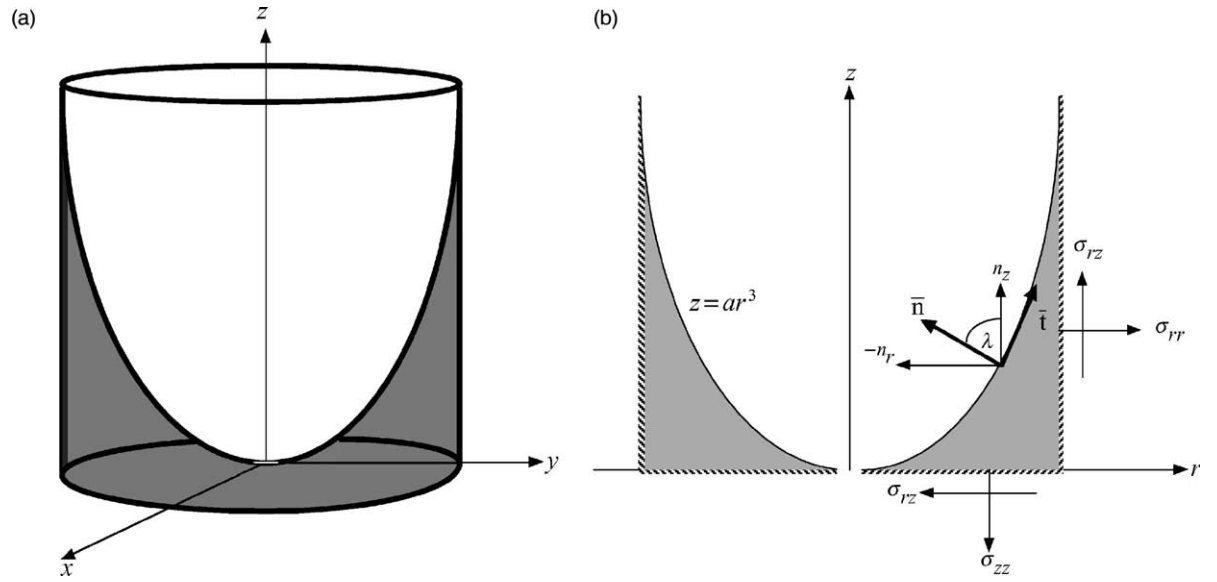

Fig. 2. (a) Three-dimensional visualisation of the cubic rat-hole occurring within a cylindrical bin. (b) Coordinates for the three-dimensional cubical rat-hole showing stresses on the base and on the cylindrical surface of the bin.

Table 1
Measured values of ϕ_e and $\sin\phi_e$ for certain granular materials, where ϕ_e is the effective angle of internal friction

Granular material	Measured of ϕ_e	$\mathrm{Sin}\,\phi_e$
Coal	69.82, 73.24, 76.62	0.938, 0.957, 0.973
Alumina filter cake	70.14	0.94
Waste rock	76.91	0.974
Silica	78.34	0.979

some variation with height, and we refer the reader to Hill and Cox (2001a) for details. Here, we are primarily concerned with the determination of the stress profile within an existing defined rat-hole. Hill and Cox (2001a), have presented analytical expressions for the stress profile for slightly tapered cylindrical cavities. Approximate stress and velocity solutions for gravity flow within tapering channels and tubes have been given by Spencer and Bradley (1992, 2002). Hill and Cox (2002a) have extended existing rat-hole theory to include granular materials which satisfy the more general shear-index yield condition. Recently, Cox et al. (submitted for publication) has determined analytical exact solutions for two and three-dimensional sloping rat-holes in highly frictional granular solids. Here, we solve the corresponding problems, but for rat-holes of parabolic and cubic profiles as indicated in Figs. 1 and 2.

Jenike (1962a, 1964, 1965) and Johanson (1964) examine radial flow solutions for which the equilibrium equations and the Coulomb–Mohr yield condition reduce to give two highly non-linear coupled ordinary differential equations for the determination of the stress field. These solutions have been re-examined by Bradley (1991) and Spencer and Bradley (1996). In general, the two highly non-linear coupled ordinary differential equations can only be solved numerically. However, based on the assumption that the angle of internal friction $\phi = 90°$, or $\beta = 1$ where $\beta = \sin\phi$, an exact parametric solution for flow from a two-dimensional converging wedge shaped hopper has been derived analytically (Hill and Cox, 2001b). Furthermore, essentially the same exact parametric solution has been exploited for the stress distribution

beneath a two-dimensional wedge shaped sand-pile (Hill and Cox, 2002b). This solution is the first exact solution of these highly non-linear coupled ordinary differential equations involving two arbitrary constants.

Another exact solution of these equations is obtained from the special case $\beta = -1$ and is given in Cox and Hill (2003). Although this special case is completely non-physical, the special case of $\beta = 1$ does give rise to an idealized mathematical theory, applying to those granular materials which might be termed highly frictional, such as those shown in Table 1. We comment that the data given in Table 1 refers to the effective angle of internal friction ϕ_e which is approximately between 0° and 10° in excess of the actual angle of internal friction, noting that for a cohesionless material, the effective angle of internal friction ϕ_e coincides with the angle of internal friction ϕ. In addition, the major issue here is not the actual magnitude of the angle of internal friction, but rather the proximity of the sine of the angle in relation to unity, noting that $\sin 64° = 0.9$. However, apart from Sture (1999) who reports angles of internal friction in the range of 70°–75° for materials under a confining pressure, there does not generally seem to exist any extensive published data for materials possessing effective angles of internal friction comparable to the high values reported in Table 1. We find, for example, from the Australian Standard (1996, p. 23) that black and brown coal, and from Perkins (1994, 1995) that certain highly angular dense soils, all exhibit relatively high values of the effective angle of internal friction in the range of 60°–65°, and $\sin 60° = 0.8660$ and $\sin 65° = 0.9063$.

For the mathematical solutions arising from the assumption $\phi = \pi/2$, we make the following comments. Firstly, we observe from the Coulomb–Mohr yield condition $|\tau| \leqslant c - \sigma \tan\phi$, that while $\tan\phi$ tends to infinity as ϕ tends to $\pi/2$, along the yield surface the normal component of traction σ tends to zero in such a way that the product $\sigma \tan\phi$ remains finite. Physically, this is equivalent to slip occurring along an infinite friction surface (see Lynch and Mason, 1993, 1995) with both zero normal and tangential shearing and through every point, there is a traction free surface. We emphasize that the assumption of $\phi = \pi/2$ does not correspond to a perfectly rough material where infinite friction prohibits any relative movement of contacting particles. Secondly, for the special case of $\phi = \pi/2$ the two families of generally distinct slip-planes coincide (see Section 5). Lastly, we also observe that as ϕ tends to $\pi/2$, the maximum principal stress (given by $\sigma_I = -p + q$ where p and q are the stress invariants defined by (2.3) or (2.21)) tends to zero. Accordingly, the material fails in the direction of σ_{III} ($\sigma_{III} = -p - q$), which has the larger magnitude (see also Section 5). Further, on rewriting the governing equations in the forms given by (2.11) and (2.29) for two and three dimensions, it is evident that approximate perturbation solutions involving powers of $1 - \sin\phi$, as given in (2.12) and (2.30) respectively, are possible. Such perturbation schemes would give rise to approximate analytical solutions for materials possessing angles of internal friction ϕ such that $1 - \sin\phi$ approaches zero. Thus, it is clear from (2.11) and (2.29) that the exact parametric solutions presented here are precisely the leading term of the respective perturbation schemes.

In the recent paper of Cox et al. (submitted for publication), the equilibrium equations, the Coulomb–Mohr yield condition and the assumption of the angle of internal friction $\phi = \pi/2$, reduce to give two novel non-linear partial differential equations for the determination of the stress field for the two situations of plane strain deformations and for axially symmetric deformations (see Eqs. (2.10) and (2.28)). By solving these equations, we may derive the exact analytical solutions for the stress distribution within a wedge and cone shaped rat-holes (Cox et al., submitted for publication). In addition, these equations give rise to a number of solution types which are examined in Thamwattana and Hill (2003). In particular, one of the solution types corresponds to the solutions which have been used in Hill and Cox (2001b, 2002b), Cox and Hill (2003) and Cox et al. (submitted for publication). In this paper we examine further special exact solutions of these novel equations which may be used to determine stress distributions for physically more realistic rat-hole geometries. Here, we assume rat-hole geometries comprising an upper perfect curved portion, resting on a rigid base with an infinitesimal central outlet as indicated in Figs. 1 and 2 for two and three dimensions respectively, and contained within vertical boundaries as shown.

In the following section, we briefly state the basic equations of non-dilatant double-shearing theory of granular flow for both plane and axially symmetric flows. On assuming an angle of internal friction $\phi = \pi/2$ ($\beta = 1$), we may deduce the basic governing partial differential equations for the stress and velocity profiles for both two and three dimensions. In Section 3, the exact analytical solutions of the governing equations for both plane and axially symmetries as determined respectively in Appendices A and B, are used to determine the stress profiles in rat-holes of parabolic and cubical profiles. Numerical stress profiles are shown graphically in Section 4. In the final section, the solutions for the velocity fields are illustrated graphically by showing the streamlines which represent the path of the flows together with the principal stress directions.

2. Basic equations for two and three dimensions

In the following two subsections we state briefly the basic equations of the continuum mechanical theory of granular material for quasi-static steady flow conforming to the Coulomb–Mohr yield condition for two and three dimensions.

2.1. Two-dimensional plane strain equations

In rectangular Cartesian coordinates (x, y, z) we consider the flow in the (x, y) plane, with y-axis vertically upwards. For steady quasi-static flows, the inertia terms may be neglected and therefore for plane strain conditions, the non-zero Cauchy stress components satisfy the equilibrium equations

$$\frac{\partial \sigma_{xx}}{\partial x} + \frac{\partial \sigma_{xy}}{\partial y} = 0, \quad \frac{\partial \sigma_{xy}}{\partial x} + \frac{\partial \sigma_{yy}}{\partial y} = \rho g, \tag{2.1}$$

where ρ denotes the bulk density, assumed constant, g is acceleration due to gravity and σ_{xx}, σ_{xy} and σ_{yy} denote the usual in-plane Cauchy stress components which are assumed to be positive in tension. These components can be expressed in standard form

$$\sigma_{xx} = -p + q\cos 2\psi, \quad \sigma_{yy} = -p - q\cos 2\psi, \quad \sigma_{xy} = q\sin 2\psi, \tag{2.2}$$

where p and q are the stress invariants defined by

$$p = -\tfrac{1}{2}(\sigma_{xx} + \sigma_{yy}), \quad q = \tfrac{1}{2}\{(\sigma_{xx} - \sigma_{yy})^2 + 4\sigma_{xy}^2\}^{1/2}, \tag{2.3}$$

while the stress angle ψ, which is the angle between the maximum principal stress and the x-axis, is given by

$$\tan 2\psi = \frac{2\sigma_{xy}}{(\sigma_{xx} - \sigma_{yy})}. \tag{2.4}$$

The stress relations are completed with the assumption of the Coulomb–Mohr yield condition

$$q = p\sin\phi + c\cos\phi, \tag{2.5}$$

where ϕ denotes the angle of internal friction and c denotes the cohesion, both of which are assumed to be constants. The above equations are generally accepted as a reasonable basis for the determination of the stress components.

On substitution of (2.2) and (2.5) into (2.1), we obtain

$$\begin{aligned} q_x &= \frac{\beta}{\beta^2 - 1}\{\rho g\beta\sin 2\psi + 2q[\psi_x \sin 2\psi - \psi_y(\beta + \cos 2\psi)]\}, \\ q_y &= \frac{\beta}{\beta^2 - 1}\{\rho g(1 - \beta\cos 2\psi) + 2q[\psi_x(\beta - \cos 2\psi) - \psi_y \sin 2\psi]\}, \end{aligned} \tag{2.6}$$

where $\beta = \sin\phi$. From (2.6) it is clear that $\beta = \pm 1$ give rise to the special cases. We rewrite (2.6) in the form

$$\begin{aligned}(\beta-1)(q_x\cos\psi + q_y\sin\psi) &= \rho g\beta\sin\psi + 2\beta q(\psi_x\sin\psi - \psi_y\cos\psi),\\ (\beta+1)(q_x\sin\psi - q_y\cos\psi) &= \rho g\beta\cos\psi - 2\beta q(\psi_x\cos\psi + \psi_y\sin\psi),\end{aligned} \tag{2.7}$$

and in particular when $\beta = 1$ it follows from $(2.7)_1$ that q is given explicitly by

$$q = -\frac{\rho g}{2}\frac{1}{(\psi_x - \psi_y\cot\psi)}, \tag{2.8}$$

while from $(2.7)_2$ for $\beta = 1$ we have

$$2(q\sin\psi)_x = \rho g\cos\psi + 2(q\cos\psi)_y, \tag{2.9}$$

and on substitution of (2.8) into (2.9) and simplifying, we obtain the novel non-linear partial differential equation

$$h_{xx} - 2hh_{xy} + h^2h_{yy} = 0, \tag{2.10}$$

where $h(x,y) = \cot\psi$. We observe that in the other special case of $\beta = -1$, we may deduce the same Eq. (2.10) in a similar manner but where $h(x,y) = -\tan\psi$. Since this case is non-physical, it will not be discussed here. We note that Eqs. (2.7) can be rewritten as

$$\begin{aligned}\rho g\sin\psi + 2q(\psi_x\sin\psi - \psi_y\cos\psi) &= (1-\beta)[\rho g\sin\psi - q_x\cos\psi - q_y\sin\psi + 2q(\psi_x\sin\psi - \psi_y\cos\psi)],\\ \rho g\cos\psi - 2(q\sin\psi)_x + 2(q\cos\psi)_y &= (1-\beta)[\rho g\cos\psi - q_x\sin\psi + q_y\cos\psi - 2q(\psi_x\cos\psi + \psi_y\sin\psi)],\end{aligned} \tag{2.11}$$

which it is clear that these equations admit perturbation solutions of the form

$$\psi = \psi_0(x,y) + \epsilon\psi_1(x,y) + \mathrm{O}(\epsilon^2), \quad q = q_0(x,y) + \epsilon q_1(x,y) + \mathrm{O}(\epsilon^2), \tag{2.12}$$

where $\epsilon = 1 - \beta$, with (2.12) satisfying (2.8) and (2.9) to leading order.

Next for the associated velocity profile, here we assume the non-dilatant double-shearing theory (Spencer, 1964, 1982). For steady flow, the non-zero velocity components $u(x,y)$ and $v(x,y)$ in the x and y directions respectively, are assumed to satisfy the equations

$$\frac{\partial u}{\partial x} + \frac{\partial v}{\partial y} = 0, \tag{2.13}$$

$$\left(\frac{\partial u}{\partial y} + \frac{\partial v}{\partial x}\right)\cos 2\psi - \left(\frac{\partial u}{\partial x} - \frac{\partial v}{\partial y}\right)\sin 2\psi + \sin\phi\left(\frac{\partial u}{\partial y} - \frac{\partial v}{\partial x} + 2\Omega\right) = 0, \tag{2.14}$$

where for steady flow Ω is defined by

$$\Omega = u\frac{\partial\psi}{\partial x} + v\frac{\partial\psi}{\partial y}.$$

Next we introduce a stream function $\chi(x,y)$ defined by

$$u(x,y) = \chi_y, \quad v(x,y) = -\chi_x, \tag{2.15}$$

which now satisfy (2.13) automatically, and on substitution of (2.15) into (2.14) we may deduce

$$(\cos 2\psi + \beta)\chi_{yy} - 2\chi_{xy}\sin 2\psi - (\cos 2\psi - \beta)\chi_{xx} = -2\beta\frac{\partial(\psi,\chi)}{\partial(x,y)}, \tag{2.16}$$

where $\partial(\psi,\chi)/\partial(x,y)$ denotes the usual Jacobian. Here for the special case of $\beta = 1$ we may obtain

$$\chi_{yy}\cot^2\psi - 2\chi_{xy}\cot\psi + \chi_{xx} = -\mathrm{cosec}^2\psi\frac{\partial(\psi,\chi)}{\partial(x,y)}, \tag{2.17}$$

and in terms of $h(x,y) = \cot\psi$ this equation becomes

$$\chi_{xx} - 2h\chi_{xy} + h^2\chi_{yy} = \frac{\partial(h,\chi)}{\partial(x,y)}. \tag{2.18}$$

2.2. Three-dimensional axially symmetric equations

In terms of cylindrical polar coordinates (r,θ,z) we consider steady quasi-static axially symmetric flow with the z-axis vertically upwards. In this case the non-zero components of the stress tensor satisfy the equilibrium equations

$$\frac{\partial\sigma_{rr}}{\partial r} + \frac{\partial\sigma_{rz}}{\partial z} + \frac{\sigma_{rr}-\sigma_{\theta\theta}}{r} = 0, \quad \frac{\partial\sigma_{rz}}{\partial r} + \frac{\partial\sigma_{zz}}{\partial z} + \frac{\sigma_{rz}}{r} = \rho g, \tag{2.19}$$

where ρ denotes the bulk solid density, assumed constant, g is the acceleration due to gravity and σ_{rr}, σ_{rz}, σ_{zz} and $\sigma_{\theta\theta}$ denote the usual physical Cauchy stress components which are assumed to be positive in tension. Again, these components can be expressed in the standard form

$$\sigma_{rr} = -p + q\cos 2\psi, \quad \sigma_{zz} = -p - q\cos 2\psi, \quad \sigma_{rz} = q\sin 2\psi, \tag{2.20}$$

where the stress invariants p, q and the stress angle ψ are defined by

$$p = -\tfrac{1}{2}(\sigma_{rr}+\sigma_{zz}), \quad q = \tfrac{1}{2}\{(\sigma_{rr}-\sigma_{zz})^2 + 4\sigma_{rz}^2\}^{1/2}, \tag{2.21}$$

$$\tan 2\psi = \frac{2\sigma_{rz}}{(\sigma_{rr}-\sigma_{zz})}. \tag{2.22}$$

For a granular material with cohesion, the stress relations are completed with the assumption of the Coulomb–Mohr yield condition (2.5). The above relations are generally accepted as a reasonable basis for the determination of the stress components. Further, we need to assume a stress state corresponding to one of the Haar–von Karman regimes, which here we adopt

$$\sigma_{\theta\theta} = -p + q. \tag{2.23}$$

On substitution of (2.5), (2.20) and (2.23) into (2.19), we obtain

$$\begin{aligned} q_r &= \frac{\beta}{\beta^2-1}\left\{\rho g\beta\sin 2\psi + 2q[\psi_r\sin 2\psi - \psi_z(\beta+\cos 2\psi)] + \frac{1}{r}q(\beta-1)(\cos 2\psi - 1)\right\},\\ q_z &= \frac{\beta}{\beta^2-1}\left\{\rho g(1-\beta\cos 2\psi) + 2q[\psi_r(\beta-\cos 2\psi) - \psi_z\sin 2\psi] + \frac{1}{r}q(\beta-1)\sin 2\psi\right\}, \end{aligned} \tag{2.24}$$

where $\beta = \sin\phi$. From (2.24) it is again clear that special cases arise from $\beta = \pm 1$. We again rewrite (2.24) in the form

$$\begin{aligned} &(\beta-1)(q_r\cos\psi + q_z\sin\psi) = \rho g\beta\sin\psi + 2\beta q(\psi_r\sin\psi - \psi_z\cos\psi),\\ &(\beta+1)(q_r\sin\psi - q_z\cos\psi) = \rho g\beta\cos\psi - 2\beta q\left(\psi_r\cos\psi + \psi_z\sin\psi + \frac{1}{r}\sin\psi\right), \end{aligned} \tag{2.25}$$

so that for the special case of $\beta = 1$, it follows from $(2.25)_1$ that q is given explicitly by

$$q = -\frac{\rho g}{2}\frac{1}{(\psi_r - \psi_z \cot\psi)}, \tag{2.26}$$

while from $(2.25)_2$ for $\beta = 1$ we find

$$2(q\sin\psi)_r = \rho g\cos\psi + 2(q\cos\psi)_z - \frac{2q}{r}\sin\psi, \tag{2.27}$$

and on substitution of (2.26) into (2.27) and simplifying, we obtain

$$h_{rr} - 2hh_{rz} + h^2 h_{zz} - \frac{1}{r}(h_r - hh_z) = 0, \tag{2.28}$$

where $h(r,z) = \cot\psi$. We observe that in the special case $\beta = -1$ which arises from assuming $\sigma_{\theta\theta} = -(p+q)$, we may deduce (2.28) in a similar manner, but where $h(r,z) = -\tan\psi$. Again this is non-physical and this case will not be discussed here. We note that Eq. (2.25) can be rewritten as

$$\begin{aligned}
&\rho g\sin\psi + 2q(\psi_r\sin\psi - \psi_z\cos\psi) = (1-\beta)[\rho g\sin\psi - q_r\cos\psi - q_z\sin\psi + 2q(\psi_r\sin\psi - \psi_z\cos\psi)],\\
&\rho g\cos\psi - 2(q\sin\psi)_r + 2(q\cos\psi)_z - \frac{2q}{r}\sin\psi\\
&\quad = (1-\beta)\left[\rho g\cos\psi - q_r\sin\psi + q_z\cos\psi - 2q\left(\psi_r\cos\psi + \psi_z\sin\psi + \frac{1}{r}\sin\psi\right)\right],
\end{aligned} \tag{2.29}$$

which it is clear that these equations admit perturbation solutions of the form

$$\psi = \psi_0(r,z) + \epsilon\psi_1(r,z) + \mathrm{O}(\epsilon^2), \quad q = q_0(r,z) + \epsilon q_1(r,z) + \mathrm{O}(\epsilon^2), \tag{2.30}$$

where $\epsilon = 1 - \beta$, with (2.30) satisfying (2.26) and (2.27) to leading order.

Next for axially symmetric flow, we also assume the non-dilatant double-shearing theory (Spencer, 1964, 1982) to determine an associated velocity profile. For steady flow the non-zero velocity components $u(r,z)$ and $v(r,z)$ in the r and z directions respectively, satisfy the following equations

$$\frac{\partial u}{\partial r} + \frac{\partial v}{\partial z} + \frac{u}{r} = 0, \tag{2.31}$$

$$\left(\frac{\partial u}{\partial z} + \frac{\partial v}{\partial r}\right)\cos 2\psi - \left(\frac{\partial u}{\partial r} - \frac{\partial v}{\partial z}\right)\sin 2\psi + \sin\phi\left(\frac{\partial u}{\partial z} - \frac{\partial v}{\partial r} + 2\Omega\right) = 0, \tag{2.32}$$

where for steady flow Ω is defined by

$$\Omega = u\frac{\partial\psi}{\partial r} + v\frac{\partial\psi}{\partial z}.$$

Here the stream function $\chi(r,z)$ is defined by

$$u(r,z) = \frac{1}{r}\chi_z, \quad v(r,z) = -\frac{1}{r}\chi_r, \tag{2.33}$$

which satisfies (2.31) automatically, and on substitution of (2.33) into (2.32) we may deduce

$$(\cos 2\psi + \beta)\chi_{zz} - 2\chi_{rz}\sin 2\psi - (\cos 2\psi - \beta)\chi_{rr} + \frac{1}{r}\chi_r(\cos 2\psi - \beta) + \frac{1}{r}\chi_z\sin 2\psi = -2\beta\frac{\partial(\psi,\chi)}{\partial(r,z)}, \tag{2.34}$$

where $\partial(\psi,\chi)/\partial(r,z)$ denotes the usual Jacobian. For the special case of $\beta = 1$ we may obtain

$$\chi_{zz}\cot^2\psi - 2\chi_{rz}\cot\psi + \chi_{rr} - \frac{1}{r}\chi_r + \frac{1}{r}\chi_z\cot\psi = -\mathrm{cosec}^2\psi\frac{\partial(\psi,\chi)}{\partial(r,z)}, \tag{2.35}$$

and in terms of $h(r,z) = \cot\psi$ we have

$$\chi_{rr} - 2h\chi_{rz} + h^2\chi_{zz} - \frac{1}{r}(\chi_r - h\chi_z) = \frac{\partial(h,\chi)}{\partial(r,z)}. \tag{2.36}$$

3. The rat-hole problems

In this section we apply the two- and three-dimensional exact parametric solutions of (2.8), (2.10), (2.26) and (2.28) as derived in Appendices A and B to determine the stress profiles in parabolic and cubical shaped rat-holes (see Figs. 1 and 2) which are considered to be realistic rat-hole profiles, like those occurring in practice in various granular industries.

3.1. Two-dimensional quadratic rat-holes

Here we assume that a rat-hole occurs when material is stored between vertical rigid walls and is at rest on a rigid base, which has an infinitesimal central outlet as shown in Fig. 1. The rat-hole comprises the upper quadratic portion, which is assumed to be determined by $y = ax^2$ $(a > 0)$ and the half length of the rigid base is ℓ and the height of the boundaries is $a\ell^2$. As shown in Appendix A, Eqs. (2.8) and (2.10) admit the following exact parametric solution

$$\begin{aligned} &\cot\psi = -\frac{2}{C_2^2}x\big(I(s) + 2\mathrm{e}^{-s/2}s^{-1/2}\big), \quad q = -\frac{\rho g}{4C_2^2}\frac{\left[C_2^4 + 4x^2\big(I(s) + 2\mathrm{e}^{-s/2}s^{-1/2}\big)^2\right]}{I(s)}, \\ &y = \frac{x^2\big(s^{-1}I(s) + I(s) + 2\mathrm{e}^{-s/2}s^{-1/2}\big)}{C_2^2}, \quad I(s) = \int^s \mathrm{e}^{-\omega/2}\omega^{-1/2}\mathrm{d}\omega + C_1, \end{aligned} \tag{3.1}$$

where C_1 and C_2 denote arbitrary constants. In order to apply the two-dimensional exact parametric solution (3.1) to determine stress profiles in two-dimensional parabolic rat-hole with a central outlet, we first need to determine the appropriate boundary conditions.

For the stress free condition along the surface of the rat-hole, we require both the tangential and normal stresses to vanish, namely

$$\sigma_t = \sigma_y\sin\lambda + \sigma_x\cos\lambda = 0, \quad \sigma_n = \sigma_y\cos\lambda - \sigma_x\sin\lambda = 0, \tag{3.2}$$

where λ is the angle defined in Fig. 1, while σ_x and σ_y denote respectively the horizontal and vertical components of the stress vector defined by

$$\sigma_x = \sigma_{xx}n_x + \sigma_{xy}n_y, \quad \sigma_y = \sigma_{xy}n_x + \sigma_{yy}n_y, \tag{3.3}$$

and n_x and n_y denote the corresponding components of the normal to the surface, and note that $\tan\lambda = -n_x/n_y$. On assuming the surface of the rat-hole is defined by $y = ax^2$ thus we have

$$n_x = -\frac{2ax}{(1+4a^2x^2)^{1/2}}, \quad n_y = \frac{1}{(1+4a^2x^2)^{1/2}},$$

from which we obtain $\lambda = \tan^{-1}(2ax)$. On substitution of (2.2) and (2.5) (assuming $\phi = 90°$) into (3.2) we may deduce the boundary condition along the surface of the rat-hole, namely $\psi = \tan^{-1}(2ax) \pm \pi/2$, which can be simplified to obtain

$$-\cot\psi = 2ax. \tag{3.4}$$

Next for convenience we introduce C_3 such that

$$I(s) = \int_0^s \mathrm{e}^{-\omega/2}\omega^{-1/2}\mathrm{d}\omega + C_3, \tag{3.5}$$

and upon letting $s = s_1$ as the parameter value along the base ($y = 0$), we obtain from $(3.1)_3$

$$I(s_1) = -\frac{2e^{-s_1/2}s_1^{1/2}}{(s_1+1)}, \tag{3.6}$$

which evidently implies that the constant C_3 must be negative. Next we introduce $s = s_2$ as the parameter value along the rat-hole surface. On substitution of (3.4) into the two-dimensional exact parametric solution (3.1), we find that $(3.1)_1$ gives

$$aC_2^2 = I(s_2) + 2e^{-s_2/2}s_2^{-1/2}, \tag{3.7}$$

and along the curve $y = ax^2$ which is the surface of the rat-hole, we also have from $(3.1)_3$ that

$$aC_2^2 = s_2^{-1}I(s_2) + I(s_2) + 2e^{-s_2/2}s_2^{-1/2}, \tag{3.8}$$

thus from (3.7) and (3.8) we may deduce $s_2^{-1}I(s_2) = 0$, which gives either $s_2 = \infty$ or $I(s_2) = 0$. We note that these two conditions cannot be true simultaneously, for otherwise $aC_2^2 = 0$. From $(3.1)_2$, in order for q to be finite, we are unable to adopt $I(s_2) = 0$ and thus we have $s_2 = \infty$ which, together with (3.7) and (3.8) becomes

$$aC_2^2 = I(\infty). \tag{3.9}$$

Now in order to determine the four constants a, s_1, C_2 and C_3, and since we cannot satisfy pointwise stress conditions at the boundaries, we assume that there are effective frictional coefficients μ_1 and μ_2 along the vertical boundary and along the base respectively such that $F_1 = \mu_1 N_1$ and $F_2 = \mu_2 N_2$ where

$$\begin{aligned}
F_1 &= \int_0^{a\ell^2} \sigma_{xy}\,dy = -\frac{\rho g}{3C_2^2}\ell^3\left(\frac{4e^{-s_1/2}s_1^{-3/2}}{(s_1+1)} - I(\infty)\right),\\
N_1 &= \int_0^{a\ell^2} \sigma_{xx}\,dy = -\frac{\rho g}{2}\ell^2\frac{1}{s_1},\\
F_2 &= \int_0^{\ell} \sigma_{xy}\,dx = -\frac{\rho g}{2}\ell^2\frac{1}{s_1},\\
N_2 &= \int_0^{\ell} \sigma_{yy}\,dx = -\frac{4}{3}\frac{\rho g}{C_2^2}\ell^3\frac{e^{-s_1/2}s_1^{-3/2}}{(s_1+1)}.
\end{aligned} \tag{3.10}$$

Now from $F_1 = \mu_1 N_1$ we may deduce

$$I(\infty) = \frac{4e^{-s_1/2}s_1^{-3/2}}{(s_1+1)} - \frac{3C_2^2\mu_1}{2\ell s_1}, \tag{3.11}$$

and from $F_2 = \mu_2 N_2$ we may obtain

$$C_2^2 = \frac{8}{3}\mu_2\ell\frac{e^{-s_1/2}s_1^{-1/2}}{(s_1+1)}, \tag{3.12}$$

so that on substitution of C_2^2 into (3.11) we may deduce

$$I(\infty) = \frac{4e^{-s_1/2}s_1^{-3/2}}{(s_1+1)}(1-\mu_1\mu_2), \tag{3.13}$$

and further on substitution of (3.12) and (3.13) into (3.9) we obtain

$$a = \frac{3}{2\ell s_1}\frac{(1-\mu_1\mu_2)}{\mu_2}. \tag{3.14}$$

Next in order to determine C_3 we rewrite $I(s)$ which is defined in (3.5) in terms of an error function thus from (3.6) and (3.13) respectively, we may deduce the following equations

$$\begin{aligned}\sqrt{2\pi}\mathrm{erf}(s_1/2)^{1/2}+C_3&=-\frac{2\mathrm{e}^{-s_1/2}s_1^{1/2}}{(s_1+1)},\\ \sqrt{2\pi}+C_3&=\frac{4\mathrm{e}^{-s_1/2}s_1^{-3/2}}{(s_1+1)}(1-\mu_1\mu_2),\end{aligned}\tag{3.15}$$

which by subtracting these two equations we may obtain the transcendental equation for s_1, namely

$$\sqrt{2\pi}-\sqrt{2\pi}\mathrm{erf}(s_1/2)^{1/2}=\frac{4\mathrm{e}^{-s_1/2}s_1^{-3/2}}{(s_1+1)}(1-\mu_1\mu_2)+\frac{2\mathrm{e}^{-s_1/2}s_1^{1/2}}{(s_1+1)}.\tag{3.16}$$

On rewriting (3.16) as

$$\mu_1\mu_2=1-\frac{1}{4}\mathrm{e}^{s_1/2}s_1^{3/2}(s_1+1)\left(\sqrt{2\pi}-\sqrt{2\pi}\mathrm{erf}(s_1/2)^{1/2}-2\frac{\mathrm{e}^{-s_1/2}s_1^{1/2}}{(s_1+1)}\right),$$

so that the effective frictional coefficients μ_1 and μ_2 must satisfy the inequalities $0<\mu_1\mu_2<1$.

3.2. Three-dimensional cubic rat-holes

Here we assume that a stable rat-hole occurs when material is stored within a cylindrical bin which has infinitesimal central outlet at the base as shown in Fig. 2. The rat-hole is assumed to comprise an upper cubic portion which is defined by $z=ar^3$ $(a>0)$ and contained within a cylindrical bin of radius ℓ so that the height is $a\ell^3$. As shown in Appendix B, Eqs. (2.26) and (2.28) admit the following exact parametric solution

$$\begin{aligned}&\cot\psi=-\frac{3}{C_2^3}r^2\left(I(s)+3\mathrm{e}^{-s/3}s^{-2/3}\right),\quad q=-\frac{\rho g}{12C_2^3}\frac{\left[C_2^6+9r^4\left(I(s)+3\mathrm{e}^{-s/3}s^{-2/3}\right)^2\right]}{rI(s)},\\ &z=\frac{r^3\left(2s^{-1}I(s)+I(s)+3\mathrm{e}^{-s/3}s^{-2/3}\right)}{C_2^3},\quad I(s)=\int^s\mathrm{e}^{-\omega/3}\omega^{-2/3}\,\mathrm{d}\omega+C_1,\end{aligned}\tag{3.17}$$

where C_1 and C_2 denote arbitrary constants. In order to apply the three-dimensional exact parametric solution (3.17) to determine the stress profile in the three-dimensional cubic rat-hole occurring in the cylindrical bin with a central outlet, we first need to determine the appropriate boundary conditions.

Following the two-dimensional solution, for the stress free condition along the surface of the rat-hole, we require both the tangential and normal stresses to vanish, namely

$$\sigma_t=\sigma_z\sin\lambda+\sigma_r\cos\lambda=0,\quad \sigma_n=\sigma_z\cos\lambda-\sigma_r\sin\lambda=0,\tag{3.18}$$

where λ is the angle defined in Fig. 2(b), while σ_r and σ_z denote the radial and vertical components of the stress vector in the cylindrical coordinate system and which are given by

$$\sigma_r=\sigma_{rr}n_r+\sigma_{rz}n_z,\quad \sigma_z=\sigma_{rz}n_r+\sigma_{zz}n_z,\tag{3.19}$$

where n_r and n_z denote the corresponding components of the normal to the surface, noting that $\tan\lambda=-n_r/n_z$. On assuming that the surface of the rat-hole is defined by $z=ar^3$, we may deduce

$$n_r=-\frac{3ar^2}{(1+9a^2r^4)^{1/2}},\quad n_z=\frac{1}{(1+9a^2r^4)^{1/2}},$$

which gives rise $\lambda = \tan^{-1}(3ar^2)$. On substitution of (2.5) and (2.20) with the assumption of $\phi = 90^\circ$ into (3.18) we may deduce that the boundary condition along the surface of the rat-hole, becomes $\psi = \tan^{-1}(3ar^2) \pm \pi/2$, which can be simplified to obtain

$$-\cot\psi = 3ar^2. \tag{3.20}$$

Next we introduce C_3 such that

$$I(s) = \int_0^s \mathrm{e}^{-\omega/3}\omega^{-2/3}\mathrm{d}\omega + C_3, \tag{3.21}$$

and upon letting $s = s_1$ be the parameter value on the base where $z = 0$, we have from $(3.17)_3$ that

$$I(s_1) = -\frac{3\mathrm{e}^{-s_1/3}s_1^{1/3}}{(s_1+2)}, \tag{3.22}$$

which again implies that the constant C_3 must be negative. Next we introduce $s = s_2$ as the parameter value on the rat-hole surface. On substitution of (3.20) into the three-dimensional exact parametric solution (3.17), we find that $(3.17)_1$ gives

$$aC_2^3 = I(s_2) + 3\mathrm{e}^{-s_2/3}s_2^{-2/3}, \tag{3.23}$$

and on the surface of the rat-hole $z = ar^3$, we also have from $(3.17)_3$ that

$$aC_2^3 = 2s_2^{-1}I(s_2) + I(s_2) + 3\mathrm{e}^{-s_2/3}s_2^{-2/3}, \tag{3.24}$$

thus from (3.23) and (3.24) we may deduce $s_2^{-1}I(s_2) = 0$ which gives either $s_2 = \infty$ or $I(s_2) = 0$, and again we note that these two conditions cannot be true simultaneously, for otherwise $aC_2^3 = 0$. From $(3.17)_2$, q must be finite and thus $I(s_2) = 0$ is not possible. Thus, we have $s_2 = \infty$, which on using (3.23) and (3.24) becomes

$$aC_2^3 = I(\infty). \tag{3.25}$$

Now in order to determine the constants a, s_1, C_2 and C_3, since we cannot satisfy pointwise stress conditions at the boundaries, we assume that there are effective frictional coefficients μ_1 and μ_2 on the surface and on the base of the cylindrical bin respectively, such that $F_1 = \mu_1 N_1$ and $F_2 = \mu_2 N_2$ where

$$\begin{aligned}
F_1 &= \int_{\theta=0}^{\theta=2\pi}\int_{z=0}^{z=a\ell^3} \ell\sigma_{rz}\,\mathrm{d}z\,\mathrm{d}\theta = -\frac{2\pi\rho g}{5C_2^3}\ell^5\left(\frac{18\mathrm{e}^{-s_1/3}s_1^{-5/3}}{(s_1+2)} - I(\infty)\right),\\
N_1 &= \int_{\theta=0}^{\theta=2\pi}\int_{z=0}^{z=a\ell^3} \ell\sigma_{rr}\,\mathrm{d}z\,\mathrm{d}\theta = -\frac{2\pi\rho g}{3}\ell^3\frac{1}{s_1},\\
F_2 &= \int_{\theta=0}^{\theta=2\pi}\int_{r=0}^{r=\ell} r\sigma_{rz}\,\mathrm{d}r\,\mathrm{d}\theta = -\frac{2\pi\rho g}{3}\ell^3\frac{1}{s_1},\\
N_2 &= \int_{\theta=0}^{\theta=2\pi}\int_{r=0}^{r=\ell} r\sigma_{zz}\,\mathrm{d}r\,\mathrm{d}\theta = -\frac{36\pi}{5}\frac{\rho g}{C_2^3}\ell^5\frac{\mathrm{e}^{-s_1/3}s_1^{-5/3}}{(s_1+2)}.
\end{aligned} \tag{3.26}$$

Now from $F_1 = \mu_1 N_1$ we may deduce

$$I(\infty) = \frac{18\mathrm{e}^{-s_1/3}s_1^{-5/3}}{(s_1+2)} - \frac{5C_2^3\mu_1}{3\ell^2 s_1} \tag{3.27}$$

and from $F_2 = \mu_2 N_2$ we may obtain

$$C_2^3 = \frac{54}{5}\mu_2 \ell^2 \frac{\mathrm{e}^{-s_1/3} s_1^{-2/3}}{(s_1+2)}, \tag{3.28}$$

so that on substitution of C_2^3 into (3.27) we find

$$I(\infty) = \frac{18\mathrm{e}^{-s_1/3} s_1^{-5/3}}{(s_1+2)}(1-\mu_1\mu_2), \tag{3.29}$$

while on substitution of (3.28) and (3.29) into (3.25) we obtain

$$a = \frac{5}{3\ell^2 s_1}\frac{(1-\mu_1\mu_2)}{\mu_2}. \tag{3.30}$$

Next to determine C_3 from (3.22) and (3.29) respectively we have

$$\begin{aligned} \int_0^{s_1} \mathrm{e}^{-\omega/3}\omega^{-2/3}\,\mathrm{d}\omega + C_3 &= -\frac{3\mathrm{e}^{-s_1/3} s_1^{1/3}}{(s_1+2)}, \\ \int_0^{\infty} \mathrm{e}^{-\omega/3}\omega^{-2/3}\,\mathrm{d}\omega + C_3 &= \frac{18\mathrm{e}^{-s_1/3} s_1^{-5/3}}{(s_1+2)}(1-\mu_1\mu_2), \end{aligned} \tag{3.31}$$

which by subtracting these two equations we may obtain the transcendental equation for s_1, namely

$$\int_{s_1}^{\infty} \mathrm{e}^{-\omega/3}\omega^{-2/3}\,\mathrm{d}\omega = \frac{18\mathrm{e}^{-s_1/3} s_1^{-5/3}}{(s_1+2)}(1-\mu_1\mu_2) + \frac{3\mathrm{e}^{-s_1/3} s_1^{1/3}}{(s_1+2)}. \tag{3.32}$$

On rewriting this equation as

$$\mu_1\mu_2 = 1 - \frac{1}{18}\mathrm{e}^{s_1/3} s_1^{5/3}(s_1+2)\left(\int_{s_1}^{\infty} \mathrm{e}^{-\omega/3}\omega^{-2/3}\,\mathrm{d}\omega - 3\frac{\mathrm{e}^{-s_1/3} s_1^{1/3}}{(s_1+2)}\right),$$

so that the effective frictional coefficients μ_1 and μ_2 must satisfy $0 < \mu_1\mu_2 < 1$.

4. Numerical results

In this section we illustrate graphically the parametric solutions for both two and three dimensional curved rat-holes. For the two-dimensional problem, on prescribing $\mu_1 = \mu_2 = \tan\pi/6$ we obtain from (3.16) $s_1 = 11.1453$, and on letting $\ell = 1$ we have from (3.12), (3.14) and (3.15) that $C_2^2 = 0.0001443$, $a = 0.1554$ and $C_3 = -2.5066$. Fig. 3 shows the variation of the stresses, σ_t, σ_n, σ_x and σ_y with y/x^2. It is clear from this figure that at $y/x^2 = a$ which corresponds to the free surface of the rat-hole, the value of all stresses are effectively zero, showing that the free surface condition is satisfied. Similarly, for the three-dimensional problem, we prescribe $\mu_1 = \tan\pi/4$ and $\mu_2 = \tan\pi/7$, so that from (3.32) we obtain $s_1 = 10.0126$, and on letting $\ell = 1$ we have from (3.28), (3.30) and (3.31) that $C_2^3 = 0.00331$, $a = 0.1792$ and $C_3 = -3.8631$. Fig. 4 shows the variation of the stresses, σ_t, σ_n, σ_r and σ_z with z/r^3. Again, it is clear from this figure that at $z/r^3 = a$ which corresponds to the free surface of the rat-hole, the value of all stresses are effectively zero, showing that the free surface condition is satisfied.

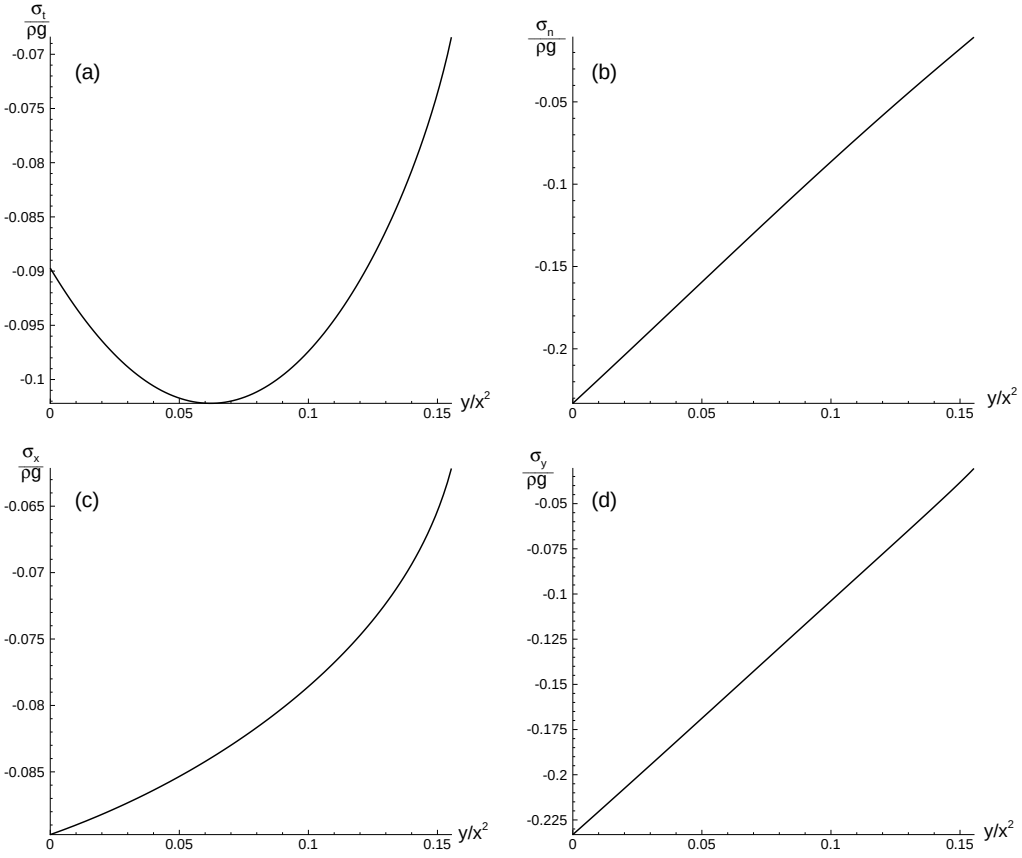

Fig. 3. Variation of the stresses, (a) σ_t, (b) σ_n, (c) σ_x and (d) σ_y with y/x^2.

5. Streamlines and failure lines

In this section we illustrate the exact solutions for the velocity fields for both plane and axially symmetric flows, by showing the streamlines, which are the particle paths, and the directions of the minimum principal stress σ_{III}. For the special case of $\phi = 90°$, the two families of slip-lines (characteristics) coalesce, and both have the direction $\mathrm{d}y/\mathrm{d}x = -\cot\psi$ in plane strain, or $\mathrm{d}z/\mathrm{d}r = -\cot\psi$ in axially symmetry. The directions of the principal stresses σ_{I} and σ_{III} are respectively determined by

$$\frac{\mathrm{d}y}{\mathrm{d}x} = \tan\psi, \quad \frac{\mathrm{d}y}{\mathrm{d}x} = -\cot\psi, \tag{5.1}$$

and similarly for the axially symmetric case,

$$\frac{\mathrm{d}z}{\mathrm{d}r} = \tan\psi, \quad \frac{\mathrm{d}z}{\mathrm{d}r} = -\cot\psi. \tag{5.2}$$

These show that the direction of the characteristics coincide with the direction of σ_{III}. This is because σ_{III} has the larger magnitude, and therefore the material fails in the direction of σ_{III}. Further, by showing the particle paths or the streamlines, it can be seen that for these flows the particles paths are in the direction of σ_{III} which might be expected.

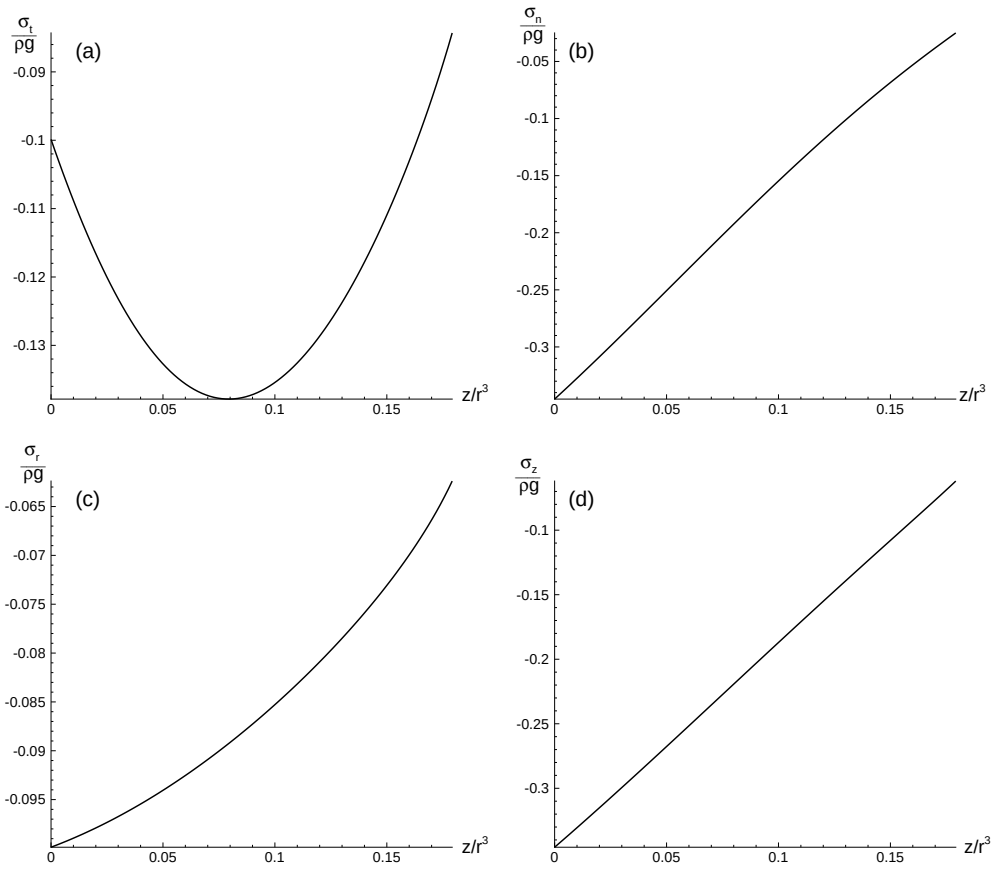

Fig. 4. Variation of the stresses, (a) σ_t, (b) σ_n, (c) σ_r and (d) σ_z with z/r^3.

5.1. Plane strain solution

From the solution $(3.1)_1$ and (5.1) we may deduce

$$\frac{\mathrm{d}y}{\mathrm{d}x} = -\frac{C_2^2}{2x(I(s)+2\mathrm{e}^{-s/2}s^{-1/2})}, \quad \frac{\mathrm{d}y}{\mathrm{d}x} = \frac{2}{C_2^2}x\big(I(s)+2\mathrm{e}^{-s/2}s^{-1/2}\big). \tag{5.3}$$

On using $(3.1)_3$ we may deduce

$$\frac{\mathrm{d}y}{\mathrm{d}x} = \frac{2}{C_2^2}x\big(s^{-1}I(s)+I(s)+2\mathrm{e}^{-s/2}s^{-1/2}\big) - \frac{x^2}{C_2^2}\frac{I(s)}{s^2}\frac{\mathrm{d}s}{\mathrm{d}x}, \tag{5.4}$$

so that on substitution of $(5.3)_{1,2}$ respectively into (5.4) we may readily deduce two differential equations, the second of which integrates, so that altogether we have

$$\frac{C_2^4+4x^2\big(s^{-1}I(s)+I(s)+2\mathrm{e}^{-s/2}s^{-1/2}\big)\big(I(s)+2\mathrm{e}^{-s/2}s^{-1/2}\big)}{(I(s)+2\mathrm{e}^{-s/2}s^{-1/2})} = 2x^3\frac{I(s)}{s^2}\frac{\mathrm{d}s}{\mathrm{d}x}, \tag{5.5}$$

and

$$C = \frac{x}{s^{1/2}}, \tag{5.6}$$

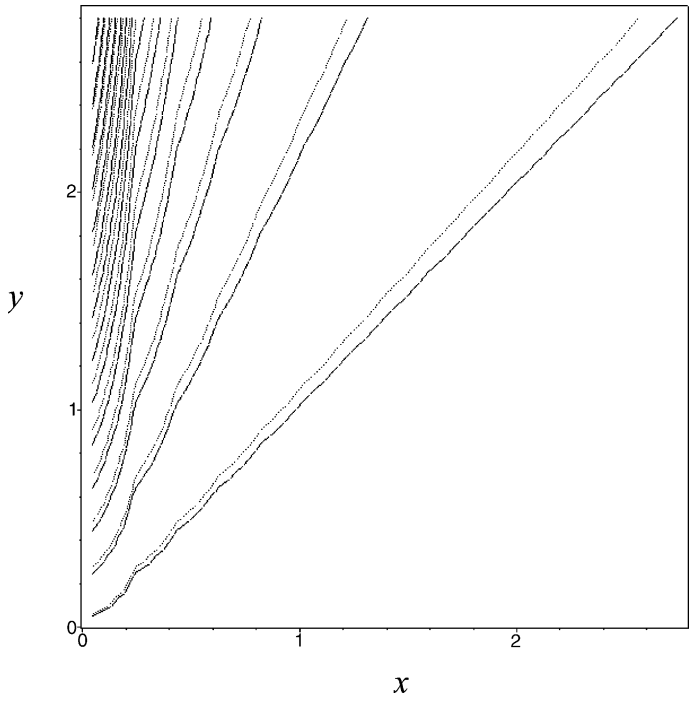

Fig. 5. Particle paths (—) and failure lines $(\cdots)$ for the plane strain solution with $\chi(x,y) = xg(x/y^{1/2})$ as determined from (5.7).

where C denotes the constant of integration. We note that Eq. (5.5) appears not to be readily integrated analytically, and we do not proceed further with this equation. The directions of σ_{III} $(\cdots)$ which are the contours of (5.6) are shown in Fig. 5 with the streamlines (—) of the stream function $\chi(x,y) = xg(x/y^{1/2})$ where $g(x/y^{1/2})$ is determined by (see Appendix A)

$$g(x/y^{1/2}) = C_3\big(I(s) + 2\mathrm{e}^{-s/2}s^{-1/2}\big) + C_4 s^{-1/2}, \tag{5.7}$$

where in the figure the constants are taken as $C_1 = 0$ and $C_2 = C_3 = C_4 = 1$. We observe that the particle paths coincide with the directions of σ_{III} as expected.

5.2. Axially symmetric solution

From the solution $(3.17)_1$ and (5.2) we may deduce

$$\frac{\mathrm{d}z}{\mathrm{d}r} = -\frac{C_2^3}{3r^2\big(I(s) + 3\mathrm{e}^{-s/3}s^{-2/3}\big)}, \quad \frac{\mathrm{d}y}{\mathrm{d}x} = \frac{3}{C_2^3}r^2\big(I(s) + 3\mathrm{e}^{-s/3}s^{-2/3}\big). \tag{5.8}$$

On using $(3.17)_3$ we may deduce

$$\frac{\mathrm{d}z}{\mathrm{d}r} = \frac{3}{C_2^3}r^2\big(2s^{-1}I(s) + I(s) + 3\mathrm{e}^{-s/3}s^{-2/3}\big) - \frac{2}{C_2^3}r^3\frac{I(s)}{s^2}\frac{\mathrm{d}s}{\mathrm{d}r}, \tag{5.9}$$

so that on substitution of $(5.8)_{1,2}$ respectively into (5.9) we may readily deduce two differential equations, the second of which integrates, so that altogether we have

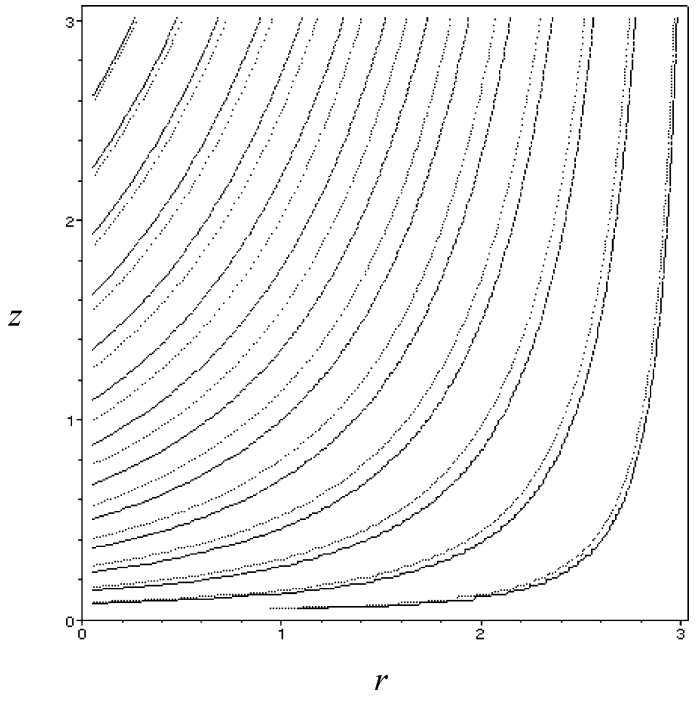

Fig. 6. Particle paths (—) and failure lines (⋯) for the axially symmetric solution with $\chi(r,z) = r^2 g(r/z^{1/3})$ as determined from (5.12).

$$\frac{C_2^6 + 9r^4\left(2s^{-1}I(s) + I(s) + 3\mathrm{e}^{-s/3}s^{-2/3}\right)\left(I(s) + 3\mathrm{e}^{-s/3}s^{-2/3}\right)}{\left(I(s) + 3\mathrm{e}^{-s/3}s^{-2/3}\right)} = 2r^5\frac{I(s)}{s^2}\frac{\mathrm{d}s}{\mathrm{d}r}, \tag{5.10}$$

and

$$C = \frac{r}{s^{1/3}}, \tag{5.11}$$

where C denotes the constant of integration. Again we note that Eq. (5.10) appears not to be readily integrated analytically, and we do not proceed further with this equation. The directions of σ_{III} (...) which are the contours of (5.11) are shown in Fig. 6 with the streamlines (—) of the stream function $\chi(r,z) = r^2 g(r/z^{1/3})$ where $g(r/z^{1/3})$ is determined by (see Appendix B)

$$g(r/z^{1/3}) = C_3\left(I(s) + 3\mathrm{e}^{-s/3}s^{-2/3}\right) + C_4 s^{-2/3}, \tag{5.12}$$

where in the figure the constants are taken as $C_1 = 0$ and $C_2 = C_3 = C_4 = 1$. We observe that the particle paths coincide with the directions of σ_{III} as expected.

6. Conclusions

On assuming the Coulomb–Mohr yield condition and the non-dilatant double-shearing theory, new exact analytical parametric solutions for both stress and velocity fields are obtained, for the special case of the angle of internal friction $\phi = 90°$. This major assumption is made primarily to facilitate an exact analytical solution. However, as discussed at length in Section 1, it may be justified principally as follows. Firstly, there exist many real materials for which the trigonometric sine of the angle of internal friction is

close to unity. This occurs for ϕ in excess of 64° (namely $\sin 64° = 0.9$). Secondly, it can be shown that for $\phi \neq \pi/2$, the general Eqs. (2.7) and (2.25) can be couched in a form (namely (2.11) and (2.29)) from which it is apparent that generally a regular perturbation solution can be found as expansions in the variable $1 - \sin\phi$ (see Eqs. (2.12) and (2.30)) with the leading term being precisely the solutions of (2.10) and (2.28) respectively. Thus, the solutions derived here may be exploited as the initial approximation in a regular perturbation series. Thirdly, we emphasize that we are not dealing with the notion of infinite friction for which no relative slip between particles is possible, but rather we are dealing here with the physical notion of slip occurring under zero normal and tangential tractions. Finally, we emphasize that for those problems which may be solved numerically for the full range $0 \leqslant \phi \leqslant \pi/2$, such as the problem of gravity flow from a hopper (Hill and Cox, 2001b) the case $\phi = \pi/2$ is seen to behave both qualitatively and quantitatively the same as other values of ϕ such as $\phi = \pi/3$ and $\pi/6$.

For the stress fields the solutions are exploited to determine the static stress distributions for highly frictional granular solids for the two and three-dimensional rat-holes which have geometries as shown in Figs. 1 and 2, and have free surfaces given respectively by $y = ax^2$ and $z = ar^3$, where a denotes a positive constant determined by (3.14) and (3.30) for two and three dimensions respectively. These solutions are bona fide exact analytical solutions for a Coulomb–Mohr granular solid and satisfy the free surface conditions on the curved upper portion, and effective frictional conditions on the boundaries. The solutions presented here are the only known analytical solutions for curved rat-hole geometries. For the associated velocity fields the particle paths, as determined from the streamlines of the stream functions for both plane and axially symmetric flows, are graphically shown together with the failure lines which coincide with the direction of the minimum principal stress σ_{III}. It is seen that the particle paths coincide with the failure lines. This is because based on the assumption of $\phi = \pi/2$ the maximum principal stress σ_{I} becomes zero, and σ_{III} has the larger magnitude and therefore the material fails in this direction.

Acknowledgements

The support from the Australian Research Council, both through the Large Grant Scheme and for providing a Senior Research Fellowship for JMH is gratefully acknowledged. The first author also gratefully acknowledges the Institute for the Promotion of teaching Science and Technology (IPST), Thailand, for financial support. The authors are also grateful to Ms. Wendy Halford, Centre for Bulk Solids and Particulate Technologies, University of Wollongong, for the data given in Table 1. The authors wish to acknowledge many illuminating discussions with Dr. Scott McCue and Dr. Grant Cox.

Appendix A. Derivation of the exact parametric solutions (3.1) and (5.7) of Eqs. (2.10) and (2.18)

In this appendix we give a brief derivation of the exact parametric solutions (3.1) and (5.7) of Eqs. (2.10) and (2.18). Eq. (2.10) gives rise to similarity solutions with functional form

$$h(x,y) = x^{(\alpha-1)} f(x/y^{1/\alpha}). \tag{A.1}$$

For general α the resulting non-linear ordinary differential equation for f appears not to admit a simple analytical solution. However, the cases $\alpha = 1$ and $\alpha = 2$ admit exact solutions in parametric form. The special case $\alpha = 1$ gives rise to the solution of the form $h(x,y) = f(x/y)$ which has been exploited to determine analytical solutions for the three problems comprising flow from a two-dimensional converging wedge shaped hopper (Hill and Cox, 2001b), secondly the stress distribution beneath a two-dimensional wedge shaped sand-pile (Hill and Cox, 2002b) and finally the stress distribution within a two-dimensional wedge rat-hole (Cox et al., submitted for publication).

For the special case $\alpha = 2$, the solution (A.1) becomes

$$h(x,y) = xf(\xi), \tag{A.2}$$

where $\xi = x/y^{1/2}$. On substitution of (A.2) into (2.10) we may obtain

$$\xi f''(\xi) + f'(\xi)\left(2 + \frac{1}{4}\frac{\xi^4 f^2(\xi)}{(1+\xi^2 f(\xi)/2)^2}\right) = 0, \tag{A.3}$$

where the prime here denotes differentiation with respect to ξ. This equation remains invariant under the stretching transformation $\xi_1 = \mathrm{e}^{\epsilon}\xi, f_1 = \mathrm{e}^{-2\epsilon}f$, and therefore we may introduce the new variable $\kappa = \xi^2 f$, so that upon making the Euler transformation $t = \ln\xi$ and $p = \kappa_t$ we obtain

$$(\kappa+2)^2 p\frac{\mathrm{d}p}{\mathrm{d}k} - 2p\{(\kappa+2)^2 + 2(\kappa+1)\} = -8\kappa(\kappa+1). \tag{A.4}$$

Now we introduce $p = 2\kappa + \eta$ into (A.4) to obtain

$$(\kappa+2)^2(2\kappa+\eta) = 4\eta(\kappa+1)\frac{\mathrm{d}\kappa}{\mathrm{d}\eta}, \tag{A.5}$$

and upon substituting $\kappa + 2 = 1/\omega$ into (A.5), we obtain

$$4\eta(\omega-1)\frac{\mathrm{d}\omega}{\mathrm{d}\eta} = 2 + (\eta-4)\omega. \tag{A.6}$$

On making the successive substitutions $\omega = v + 1$ and $v = m + \eta/4$ we may deduce the Bernouli equation

$$-(4m+2)\frac{\mathrm{d}\eta}{\mathrm{d}m} = 4\eta m + \eta^2, \tag{A.7}$$

which on solving in the usual way gives

$$\frac{1}{\eta} = \frac{\mathrm{e}^m}{2(2m+1)^{1/2}}I(m), \tag{A.8}$$

where

$$I(m) = \int \frac{\mathrm{e}^{-m}}{(2m+1)^{1/2}}\mathrm{d}m + C_1^*, \tag{A.9}$$

where C_1^* denotes the arbitrary constant.

On retracing the above transformations we find

$$\kappa = -\frac{\left(I(m) + 2mI(m) + \mathrm{e}^{-m}(2m+1)^{1/2}\right)}{(I(m) + mI(m) + \mathrm{e}^{-m}(2m+1)^{1/2}/2)},$$

$$p = 2\frac{2m\mathrm{e}^{-m}(2m+1)^{1/2}I(m) + \mathrm{e}^{-2m}(2m+1) - 2(2m+1)I^2(m)}{I(m)(2I(m) + 2mI(m) + \mathrm{e}^{-m}(2m+1)^{1/2})},$$

and from $\mathrm{d}t = \mathrm{d}\kappa/p$ and $t = \ln\xi$ we may deduce

$$t = \int^m \frac{I(m)}{(2m+1)\left(2I(m) + 2mI(m) + \mathrm{e}^{-m}(2m+1)^{1/2}\right)}\mathrm{d}m + C_2^*, \tag{A.10}$$

where C_2^* denotes a further arbitrary constant. Next we introduce $s = 2m + 1$, thus (A.10) becomes

$$\begin{aligned} t &= \frac{1}{2}\int \frac{I(s)}{s(I(s) + sI(s) + 2\mathrm{e}^{-s/2}s^{1/2})}\mathrm{d}s, \\ &= \frac{1}{2}\int \frac{I(s)}{s^2}\frac{1}{(s^{-1}I(s) + I(s) + 2\mathrm{e}^{-s/2}s^{-1/2})}\mathrm{d}s, \\ &= -\frac{1}{2}\int \frac{\mathrm{d}(s^{-1}I(s) + I(s) + 2\mathrm{e}^{-s/2}s^{-1/2})}{(s^{-1}I(s) + I(s) + 2\mathrm{e}^{-s/2}s^{-1/2})}, \\ &= \ln C_2(s^{-1}I(s) + I(s) + 2\mathrm{e}^{-s/2}s^{-1/2})^{-1/2}, \end{aligned}$$

where $I(s)$ is defined by

$$I(s) = \int^s \mathrm{e}^{-\omega/2}\omega^{-1/2}\mathrm{d}\omega + C_1, \tag{A.11}$$

and C_1 and C_2 denote new arbitrary constants. Thus from $t = \ln\xi$ where $\xi = x/y^{1/2}$ we may obtain

$$\frac{x}{y^{1/2}} = C_2(s^{-1}I(s) + I(s) + 2\mathrm{e}^{-s/2}s^{-1/2})^{-1/2}, \tag{A.12}$$

and we rewrite κ in terms of the parameter s as

$$\kappa = -2\frac{\left(sI(s) + 2\mathrm{e}^{-s/2}s^{1/2}\right)}{(I(s) + sI(s) + 2\mathrm{e}^{-s/2}s^{1/2})}. \tag{A.13}$$

Thus from (A.2) where $f = \kappa/\xi^2$ we find that the exact analytical parametric solution of (2.10) for the special case of $\alpha = 2$ becomes

$$\cot\psi = -\frac{2}{C_2^2}x\left(I(s) + 2\mathrm{e}^{-s/2}s^{-1/2}\right). \tag{A.14}$$

In order to determine q, from (A.11) and (A.14) we may deduce

$$\begin{aligned} \psi_x &= -\frac{1}{[1 + 4x^2(I(s) + 2\mathrm{e}^{-s/2}s^{-1/2})^2/C_2^4]}\left\{\frac{2}{C_2^2}s^{-3/2}\mathrm{e}^{-s/2}xs_x - \frac{2}{C_2^2}\left(I(s) + 2\mathrm{e}^{-s/2}s^{-1/2}\right)\right\}, \\ \psi_y &= -\frac{1}{[1 + 4x^2(I(s) + 2\mathrm{e}^{-s/2}s^{-1/2})^2/C_2^4]}\frac{2}{C_2^2}s^{-3/2}\mathrm{e}^{-s/2}xs_y, \end{aligned} \tag{A.15}$$

where xs_x and xs_y are derived by differentiation of (A.12) with respect to x and y respectively

$$\begin{aligned} xs_x &= 2\frac{s^2}{I(s)}\left(s^{-1}I(s) + I(s) + 2\mathrm{e}^{-s/2}s^{-1/2}\right), \\ xs_y &= -C_2^2\frac{s^2}{xI(s)}, \end{aligned} \tag{A.16}$$

and on substitution of (A.15) and (A.16) into (2.8) and simplifying we may deduce

$$q = -\frac{\rho g}{4C_2^2}\frac{\left[C_2^4 + 4x^2\left(I(s) + 2\mathrm{e}^{-s/2}s^{-1/2}\right)^2\right]}{I(s)}. \tag{A.17}$$

Next for the velocity profile, we assume $\chi(x,y) = xg(\xi)$ and on substitution into (2.18) we may deduce

$$\xi g''(\xi) + g'(\xi)\left\{2 + \frac{1}{2}\xi^2 f(\xi)\frac{1}{(1 + \xi^2 f(\xi)/2)}\right\} - \frac{1}{2}\xi^2\frac{1}{(1 + \xi^2 f(\xi)/2)^2}f'(\xi)g(\xi) = 0, \tag{A.18}$$

where the prime here denotes differentiation with respect to ξ. Eq. (A.18) is a homogeneous linear equation of the second order of the form

$$f_2(\xi)g''(\xi) + f_1(\xi)g'(\xi) + f_0(\xi)g(\xi) = 0,$$

where the general solution is given by

$$g = g_0\left(c_1 + c_2\int \frac{\mathrm{e}^{-F}}{g_0^2}\mathrm{d}\xi\right), \tag{A.19}$$

where c_1 and c_2 denote arbitrary constants, $F = \int f_1/f_2\,\mathrm{d}\xi$ and $g_0 = g_0(\xi)$ is a non-trivial particular solution which for Eq. (A.18) we may use $g_0(\xi) = f(\xi)$ where $f(\xi)$ is given by κ/ξ^2. In order to determine F we have from

$$F = \int \frac{2}{\xi}\mathrm{d}\xi + \frac{1}{2}\int \frac{\xi f(\xi)}{(1+\xi^2 f(\xi)/2)}\mathrm{d}\xi. \tag{A.20}$$

Now we consider the second integral of (A.20). From $f(\xi) = \kappa/\xi^2$ where ξ and κ are determined by (A.12) and (A.13), we obtain

$$\frac{1}{2}\int \frac{\xi f(\xi)}{(1+\xi^2 f(\xi)/2)}\mathrm{d}\xi = \int \frac{\kappa}{\xi(2+\kappa)}\mathrm{d}\xi. \tag{A.21}$$

In terms of the parameter s we may deduce

$$\begin{aligned}\int \frac{\kappa}{\xi(2+\kappa)}\mathrm{d}\xi &= -\frac{1}{2}\int \frac{(I(s) + 2\mathrm{e}^{-s/2}s^{-1/2})}{(I(s) + sI(s) + 2\mathrm{e}^{-s/2}s^{1/2})}\mathrm{d}s,\\ &= -\frac{1}{2}\int \frac{\mathrm{d}(I(s) + sI(s) + 2\mathrm{e}^{-s/2}s^{1/2})}{(I(s) + sI(s) + 2\mathrm{e}^{-s/2}s^{1/2})},\\ &= -\frac{1}{2}\ln(I(s) + sI(s) + 2\mathrm{e}^{-s/2}s^{1/2}).\end{aligned} \tag{A.22}$$

On substitution of (A.12) and (A.22) into (A.20) we deduce

$$F = \ln\frac{C_2^2 s}{(I(s) + sI(s) + 2\mathrm{e}^{-s/2}s^{1/2})^{3/2}}, \tag{A.23}$$

and from $g_0(\xi) = f(\xi) = \kappa/\xi^2$, we have

$$g_0 = -\frac{2}{C_2^2}(I(s) + 2\mathrm{e}^{-s/2}s^{-1/2}),$$

therefore

$$\int \frac{\mathrm{e}^{-F}}{g_0^2}\mathrm{d}\xi = \frac{C_2^3}{8}\int \frac{I(s)}{s^{1/2}}\frac{1}{(s^{1/2}I(s) + 2\mathrm{e}^{-s/2})^2}\mathrm{d}s. \tag{A.24}$$

Now we may rewrite the right hand side of the integral of (A.24) in the form

$$\frac{C_2^3}{8}\int \frac{I(s)}{s^{1/2}}\frac{1}{(s^{1/2}I(s) + 2\mathrm{e}^{-s/2})^2}\mathrm{d}s = \frac{C_2^3}{4}\int \frac{a'(s)}{a^2(s)}\mathrm{d}s = -\frac{C_2^3}{4}\frac{1}{a(s)} + C^*, \tag{A.25}$$

where $a(s) = s^{1/2}I(s) + 2\mathrm{e}^{-s/2}$ and C^* denotes arbitrary constant. Therefore on substitution of (A.25) into (A.24) we may deduce

Table 2
Tabulated comparison of the parametric solutions (A.1) of (2.10) and (2.18) for $\alpha = 1$ and $\alpha = 2$ where here $r = (x^2 + y^2)^{1/2}$

$\alpha = 1$	$\alpha = 2$
$h(x,y) = f(x/y)$	$h(x,y) = xf(x/y^{1/2})$
$\cot\psi = -\dfrac{I(s)}{C_2}$	$\cot\psi = -\frac{2}{C_2^2}x(I(s) + 2\mathrm{e}^{-s/2}s^{-1/2})$
$y = \dfrac{x(I(s) + 2s^{-1/2}\mathrm{e}^{-s/2})}{C_2}$	$y = \dfrac{x^2(s^{-1}I(s) + I(s) + 2\mathrm{e}^{-s/2}s^{-1/2})}{C_2^2}$
$I(s) = \int^s \omega^{-1/2}\mathrm{e}^{-\omega/2}\,\mathrm{d}\omega + C_1$	$I(s) = \int^s \omega^{-1/2}\mathrm{e}^{-\omega/2}\,\mathrm{d}\omega + C_1$
$q = \dfrac{\rho g r}{4}\dfrac{s^{-1/2}\mathrm{e}^{s/2}[C_2^2 + I^2(s)]}{\{C_2^2 + [2s^{-1/2}\mathrm{e}^{-s/2} + I(s)]^2\}^{1/2}}$	$q = -\dfrac{\rho g}{4C_2^2}\dfrac{[C_2^4 + 4x^2(I(s) + 2\mathrm{e}^{-s/2}s^{-1/2})^2]}{I(s)}$
$\chi(x,y) = g(x/y)$	$\chi(x,y) = xg(x/y^{1/2})$
$g(x/y) = C_3 I(s) + C_4$	$g(x/y^{1/2}) = C_3(I(s) + 2\mathrm{e}^{-s/2}s^{-1/2}) + C_4 s^{-1/2}$

$$\int \frac{\mathrm{e}^{-F}}{g_0^2}\,\mathrm{d}\xi = -\frac{C_2^3}{4}\frac{1}{(s^{1/2}I(s) + 2\mathrm{e}^{-s/2})} + C,$$

where C denotes further arbitrary constant. Hence, from (A.19) the general solution of (A.18) is given by

$$g(\xi) = C_3(I(s) + 2\mathrm{e}^{-s/2}s^{-1/2}) + C_4 s^{-1/2}, \tag{A.26}$$

where C_3 and C_4 denote arbitrary constants.

In order to make a comparison with the known exact parametric solutions for $\alpha = 1$ we present both parametric solutions for $\alpha = 1$ and $\alpha = 2$ for both stress and velocity profiles in Table 2.

Appendix B. Derivation of the exact parametric solutions (3.17) and (5.12) of Eqs. (2.28) and (2.36)

In this appendix we give a brief derivation of the exact parametric solutions (3.17) and (5.12) of Eqs. (2.28) and (2.36). Eq. (2.28) gives rise to similarity solutions with functional form

$$h(r,z) = r^{(\alpha-1)}f(r/z^{1/\alpha}). \tag{B.1}$$

Again for general α the resulting non-linear ordinary differential equation for f appears not to admit a simple analytical solution. However, the cases $\alpha = 1$ and $\alpha = 3$ admit exact solution in parametric form. The special case of $\alpha = 1$ gives rise to the solution of the form $h(r,z) = f(r/z)$ which has been exploited to determine analytical solution for the stress distribution within a three-dimensional conical rat-hole (Cox et al., submitted for publication).

For the special case $\alpha = 3$ the solution (B.1) becomes

$$h(r,z) = r^2 f(\xi), \tag{B.2}$$

where $\xi = r/z^{1/3}$. On substitution of (B.2) into (2.28) we may deduce

$$\xi f''(\xi) + f'(\xi)\left\{3 - \frac{1}{3}\xi^3 f(\xi)\frac{(1 - \xi^3 f(\xi)/3)}{(1 + \xi^3 f(\xi)/3)^2}\right\} = 0, \tag{B.3}$$

where the prime here denotes differentiation with respect to ξ. This equation remains invariant under the stretching transformation $\xi_1 = \mathrm{e}^{\epsilon}\xi$, $f_1 = \mathrm{e}^{-3\epsilon}f$, and therefore we introduce the new variable $\kappa = \xi^3 f$, so that upon making the Euler transformation $t = \ln\xi$, and $p = \kappa_t$ we obtain

$$(\kappa+3)^2 p\frac{\mathrm{d}p}{\mathrm{d}k} - 3p\{(\kappa+3)^2 + 3(\kappa+1)\} = -27\kappa(\kappa+1). \tag{B.4}$$

Now on introducing $p = 3\kappa + \eta$ into (B.4) we obtain

$$(\kappa+3)^2(3\kappa+\eta) = 9\eta(\kappa+1)\frac{\mathrm{d}\kappa}{\mathrm{d}\eta}, \tag{B.5}$$

and upon introducing $\kappa + 3 = 1/\omega$ into (B.5), we have

$$9\eta(2\omega-1)\frac{\mathrm{d}\omega}{\mathrm{d}\eta} = 3 + (\eta-9)\omega. \tag{B.6}$$

On making the successive substitution $\omega = (v+1)/2$ and $v = m + \eta/9$ we may deduce the Bernouli equation

$$-(9m+3)\frac{\mathrm{d}\eta}{\mathrm{d}m} = 9\eta m + \eta^2, \tag{B.7}$$

which on solving in the usual way gives

$$\frac{1}{\eta} = \frac{\mathrm{e}^m}{3(3m+1)^{1/3}} I(m), \tag{B.8}$$

where

$$I(m) = \int \frac{\mathrm{e}^{-m}}{(3m+1)^{2/3}}\,\mathrm{d}m + C_1^*, \tag{B.9}$$

where C_1^* denotes the arbitrary constant.

On retracing the above transformations we find

$$\kappa = -\frac{(I(m) + 3mI(m) + \mathrm{e}^{-m}(3m+1)^{1/3})}{(I(m) + mI(m) + \mathrm{e}^{-m}(3m+1)^{1/3}/3)},$$

$$p = 3\frac{3m\mathrm{e}^{-m}(3m+1)^{1/3}I(m) + 2\mathrm{e}^{-2m}(3m+1)^{2/3} - 3(3m+1)I^2(m)}{I(m)(3I(m) + 3mI(m) + \mathrm{e}^{-m}(3m+1)^{1/3})},$$

and from $\mathrm{d}t = \mathrm{d}\kappa/p$ and $t = \ln\xi$ we may deduce

$$t = \int^m \frac{2I(m)}{(3m+1)\left(3I(m) + 3mI(m) + \mathrm{e}^{-m}(3m+1)^{1/3}\right)}\,\mathrm{d}m + C_2^*, \tag{B.10}$$

where C_2^* denotes a further arbitrary constant. Next we introduce $s = 3m + 1$, thus (B.10) becomes

$$\begin{aligned} t &= \frac{2}{3}\int \frac{I(s)}{s(2I(s) + sI(s) + 3\mathrm{e}^{-s/3}s^{1/3})}\,\mathrm{d}s, \\ &= \frac{2}{3}\int \frac{I(s)}{s^2}\,\frac{1}{(2s^{-1}I(s) + I(s) + 3\mathrm{e}^{-s/3}s^{-2/3})}\,\mathrm{d}s, \\ &= -\frac{1}{3}\int \frac{\mathrm{d}(2s^{-1}I(s) + I(s) + 3\mathrm{e}^{-s/3}s^{-2/3})}{(2s^{-1}I(s) + I(s) + 3\mathrm{e}^{-s/3}s^{-2/3})}, \\ &= \ln C_2(2s^{-1}I(s) + I(s) + 3\mathrm{e}^{-s/3}s^{-2/3})^{-1/3}, \end{aligned}$$

where $I(s)$ is defined by

$$I(s) = \int^s \mathrm{e}^{-\omega/3}\omega^{-2/3}\mathrm{d}\omega + C_1, \tag{B.11}$$

and C_1 and C_2 denote new arbitrary constants. Thus from $t = \ln \xi$ where $\xi = r/z^{1/3}$ we may obtain

$$\frac{r}{z^{1/3}} = C_2(2s^{-1}I(s) + I(s) + 3\mathrm{e}^{-s/3}s^{-2/3})^{-1/3}, \tag{B.12}$$

and we rewrite κ in terms of the parameter s as

$$\kappa = -3\frac{\left(sI(s) + 3\mathrm{e}^{-s/3}s^{1/3}\right)}{(2I(s) + sI(s) + 3\mathrm{e}^{-s/3}s^{1/3})}. \tag{B.13}$$

Thus from (B.2) where $f = \kappa/\xi^3$ we find that the exact analytical parametric solution of (2.28) for the special case of $\alpha = 3$ becomes

$$\cot\psi = -\frac{3}{C_2^3}r^2\left(I(s) + 3\mathrm{e}^{-s/3}s^{-2/3}\right). \tag{B.14}$$

In order to determine q, from (B.11) and (B.14) we may deduce

$$\begin{aligned}
\psi_r &= -\frac{1}{[1 + 9r^4(I(s) + 3\mathrm{e}^{-s/3}s^{-2/3})^2/C_2^6]}\left\{\frac{6}{C_2^3}s^{-5/3}\mathrm{e}^{-s/3}r^2s_r - \frac{6}{C_2^3}r\left(I(s) + 3\mathrm{e}^{-s/3}s^{-2/3}\right)\right\},\\
\psi_z &= -\frac{1}{[1 + 9r^4(I(s) + 3\mathrm{e}^{-s/3}s^{-2/3})^2/C_2^6]}\frac{6}{C_2^3}s^{-5/3}\mathrm{e}^{-s/3}r^2s_z,
\end{aligned} \tag{B.15}$$

where r^2s_r and r^2s_z are derived by differentiation of (B.12) with respect to r and z respectively

$$\begin{aligned}
r^2s_r &= \frac{3}{2}r\frac{s^2}{I(s)}\left(2s^{-1}I(s) + I(s) + 3\mathrm{e}^{-s/3}s^{-2/3}\right),\\
r^2s_z &= -\frac{C_2^3}{2}\frac{s^2}{rI(s)},
\end{aligned} \tag{B.16}$$

and on substitution of (B.15) and (B.16) into (2.26) and simplifying we may deduce

$$q = -\frac{\rho g}{12C_2^3}\frac{\left[C_2^6 + 9r^4\left(I(s) + 3\mathrm{e}^{-s/3}s^{-2/3}\right)^2\right]}{rI(s)}. \tag{B.17}$$

Next for the velocity profile, we assume $\chi(r,z) = r^2g(\xi)$ and on substitution into (2.36) we may deduce

$$\xi g''(\xi) + g'(\xi)\left\{3 + \frac{1}{3}\xi^3 f(\xi)\frac{1}{(1 + \xi^3 f(\xi)/3)}\right\} - \frac{2}{3}\xi^3\frac{1}{(1 + \xi^3 f(\xi)/3)^2}f'(\xi)g(\xi) = 0, \tag{B.18}$$

where the prime denotes differentiation with respect to ξ. Eq. (B.18) is also a homogeneous linear equation of the second order where the general solution can be found from the formula (A.19). Again we may use $g_0(\xi) = f(\xi)$ where $f(\xi) = \kappa/\xi^3$. In order to determine F we have from

$$F = \int\frac{3}{\xi}\mathrm{d}\xi + \frac{1}{3}\int\frac{\xi^2 f(\xi)}{(1 + \xi^3 f(\xi)/3)}\mathrm{d}\xi. \tag{B.19}$$

Now we consider the second integral of (B.19). From $f(\xi) = \kappa/\xi^3$ where ξ and κ are determined by (B.12) and (B.13), we obtain

$$\frac{1}{3}\int\frac{\xi^2 f(\xi)}{(1 + \xi^3 f(\xi)/3)}\mathrm{d}\xi = \int\frac{\kappa}{\xi(3 + \kappa)}\mathrm{d}\xi. \tag{B.20}$$

In terms of the parameter s we may deduce

$$\begin{aligned}\int \frac{\kappa}{\xi(3+\kappa)}\,\mathrm{d}\xi &= -\frac{1}{3}\int \frac{(I(s)+3\mathrm{e}^{-s/3}s^{-2/3})}{(2I(s)+sI(s)+3\mathrm{e}^{-s/3}s^{1/3})}\,\mathrm{d}s,\\ &= -\frac{1}{3}\int \frac{\mathrm{d}(2I(s)+sI(s)+3\mathrm{e}^{-s/3}s^{1/3})}{(2I(s)+sI(s)+3\mathrm{e}^{-s/3}s^{1/3})},\\ &= -\frac{1}{3}\ln(2I(s)+sI(s)+3\mathrm{e}^{-s/3}s^{1/3}).\end{aligned} \tag{B.21}$$

On substitution of (B.12) and (B.21) into (B.19) we deduce

$$F = \ln\frac{C_2^3 s}{(2I(s)+sI(s)+3\mathrm{e}^{-s/3}s^{1/3})^{4/3}}, \tag{B.22}$$

and from $g_0(\xi) = f(\xi) = \kappa/\xi^3$ we have

$$g_0 = -\frac{3}{C_2^3}(I(s)+3\mathrm{e}^{-s/3}s^{-2/3}),$$

therefore

$$\int \frac{\mathrm{e}^{-F}}{g_0^2}\,\mathrm{d}\xi = \frac{2C_2^4}{27}\int \frac{I(s)}{s^{1/3}}\frac{1}{(s^{2/3}I(s)+3\mathrm{e}^{-s/3})^2}\,\mathrm{d}s. \tag{B.23}$$

Now we may rewrite the right hand side of the integral of (B.23) in the form

$$\frac{2C_2^4}{27}\int \frac{I(s)}{s^{1/3}}\frac{1}{(s^{2/3}I(s)+3\mathrm{e}^{-s/3})^2}\,\mathrm{d}s = \frac{C_2^4}{9}\int \frac{a'(s)}{a^2(s)}\,\mathrm{d}s = -\frac{C_2^4}{9}\frac{1}{a(s)} + C^*, \tag{B.24}$$

where $a(s) = s^{2/3}I(s) + 3\mathrm{e}^{-s/3}$ and C^* denotes arbitrary constant. Therefore on substitution of (B.24) into (B.23) we may deduce

$$\int \frac{\mathrm{e}^{-F}}{g_0^2}\,\mathrm{d}\xi = -\frac{C_2^4}{9}\frac{1}{(s^{2/3}I(s)+3\mathrm{e}^{-s/3})} + C,$$

where C denotes further arbitrary constant. Hence, from (A.19) the general solution of (B.18) is given by

$$g(\xi) = C_3(I(s)+3\mathrm{e}^{-s/3}s^{-2/3}) + C_4 s^{-2/3}, \tag{B.25}$$

where C_3 and C_4 denote arbitrary constant.

Table 3
Tabulated comparison of the parametric solutions (B.1) of (2.28) and (2.36) for $\alpha = 1$ and $\alpha = 3$ where here $R = (r^2+z^2)^{1/2}$

$\alpha = 1$	$\alpha = 3$
$h(r,z) = f(r/z)$	$h(r,z) = r^2 f(r/z^{1/3})$
$\cot\psi = -\dfrac{I(s)}{C_2}$	$\cot\psi = -\dfrac{3}{C_2^3}r^2(I(s)+3\mathrm{e}^{-s/3}s^{-2/3})$
$z = \dfrac{r(I(s)+3s^{-1/3}\mathrm{e}^{-s/3})}{C_2}$	$z = \dfrac{r^3(2s^{-1}I(s)+I(s)+3\mathrm{e}^{-s/3}s^{-2/3})}{C_2^3}$
$I(s) = \int^s \omega^{-1/3}\mathrm{e}^{-\omega/3}\,\mathrm{d}\omega + C_1$	$I(s) = \int^s \omega^{-2/3}\mathrm{e}^{-\omega/3}\,\mathrm{d}\omega + C_1$
$q = \dfrac{\rho g R}{6}\dfrac{s^{-2/3}\mathrm{e}^{s/3}[C_2^2+I^2(s)]}{\{C_2^2+[3s^{-1/3}\mathrm{e}^{-s/3}+I(s)]^2\}^{1/2}}$	$q = -\dfrac{\rho g}{12C_2^3}\dfrac{[C_2^6+9r^4(I(s)+3\mathrm{e}^{-s/3}s^{-2/3})^2]}{rI(s)}$
$\chi(r,z) = g(r/z)$	$\chi(r,z) = r^2 g(r/z^{1/3})$
$g(r/z) = C_3 I(s) + C_4$	$g(r/z^{1/3}) = C_3(I(s)+3\mathrm{e}^{-s/3}s^{-2/3}) + C_4 s^{-2/3}$

In order to make a comparison with the known exact parametric solutions for $\alpha = 1$ we present both parametric solutions for $\alpha = 1$ and $\alpha = 3$ for both stress and velocity profiles in Table 3.

References

Australian Standard, 1996. Loads on bulk solids containers. Standards Association of Australia. ISBN 0733707335, AS 3774, p. 23.

Bradley, N.J., 1991. Gravity Flows of Granular Materials. Ph.D. Thesis, University of Nottingham.

Cox, G.M., Hill, J.M., 2003. Some exact mathematical solutions for granular stock piles and granular flow in hoppers. Mathematics and Mechanics of Solids 8, 21–50.

Cox, G.M., Hill, J.M., Thamwattana, N., submitted for publication. An analytical solution for a sloping rat-hole in an highly frictional granular solid. Proc. Roy. Soc. Lond. A.

Hill, J.M., Cox, G.M., 2000. Cylindrical cavities and classical rat-hole theory occurring in bulk materials. Int. J. Numer. Anal. Meth. Geomech. 24, 971–990.

Hill, J.M., Cox, G.M., 2001a. Stress profiles for tapered cylindrical cavities in granular media. Int. J. Solids Struct. 38, 3795–3811.

Hill, J.M., Cox, G.M., 2001b. An exact parametric solution for granular flow in a converging wedge. Z. Angew. Math. Physik (ZAMP) 52, 657–668.

Hill, J.M., Cox, G.M., 2002a. Rat-hole stress profiles for shear-index granular materials. Acta Mech. 155, 157–172.

Hill, J.M., Cox, G.M., 2002b. On the problem of the determination of force distributions in granular heaps using continuum theory. Q. J. Mech. Appl. Math. 55, 655–668.

Jenike, A.W., 1962a. Gravity flow of bulk solids. Utah Engineering Experiment Station. Bulletin no. 108.

Jenike, A.W., 1962b. Gravity flow of solids. Trans. Inst. Chem. Eng. 40, 264–471.

Jenike, A.W., 1964. Steady gravity flow of frictional-cohesive solids in converging channels. J. Appl. Mech. 31, 5–11.

Jenike, A.W., 1965. Gravity flow of frictional-cohesive solids—convergence to radial stress fields. J. Appl. Mech. 32, 205–207.

Jenike, A.W., Yen, B.C., 1962a. Slope stability in axially symmetry. Utah Engineering Experiment Station. Bulletin no. 115.

Jenike, A.W., Yen, B.C., 1962b. Slope stability in axially symmetry. In: Proc. Fifth Symposium on Rock Mechanics, May 1962, University of Minnesota. Pergamon Press, New York, pp. 689–711.

Johanson, J.R., 1964. Stress and velocity fields in the gravity flow of bulk solids. J. Appl. Mech. 31, 499–506.

Lynch, K.M., Mason, M.T., 1993. Pulling by pushing, slip with infinite friction, and perfectly rough surfaces. In: Int. Conf. on Robotics and Automation, vol. 1, Atlanta, 2–6 May 1993. IEEE, pp. 745–751.

Lynch, K.M., Mason, M.T., 1995. Pulling by pushing, slip with infinite friction, and perfectly rough surfaces. Int. Rob. Res. 14, 174–183.

Perkins, S.W., 1994. Non-linear limit analysis for the bearing capacity of highly frictional soils. In: 2nd Congress on Computing in Civil Engineering, vol. 1, Atlanta, 4 June 1995. ASCE, pp. 629–636.

Perkins, S.W., 1995. Bearing capacity of highly frictional material. ASTM Geotech. Testing J. 18, 450–462.

Spencer, A.J.M., 1964. A theory of the kinematics of ideal soils under plane strain conditions. J. Mech. Phys. Solids 12, 337–351.

Spencer, A.J.M., 1982. Deformation of ideal granular materials. In: Hopkin, H.G., Sewell, M.J. (Eds.), Mechanics of Solids. Pergamon Press, Oxford, pp. 607–652.

Spencer, A.J.M., Bradley, N.J., 1992. Gravity flow of a granular material in compression between vertical walls and through a tapering vertical channel. Q. J. Mech. Appl. Math. 45, 733–746.

Spencer, A.J.M., Bradley, N.J., 1996. Gravity flow of granular materials in converging wedges and cones. In: Markov, K.Z. (Ed.), Proc. 8th Int. Sym. Continuum Models and Discrete Systems. World Scientific, Singapore, pp. 581–590.

Spencer, A.J.M., Bradley, N.J., 2002. Gravity flow of granular materials in contracting cylinders and tapered tubes. Int. J. Eng. Sci. 40, 1529–1552.

Sture, S., 1999. Constitutive issues in soil liquefaction. In: Lade, P.V., Yamamuro, J.A. (Eds.), Physics and Mechanics of Soil Liquefaction. Balkema, Rotterdam, pp. 133–143.

Thamwattana, N., Hill, J.M., 2003. Analytical stress and velocity fields for highly frictional granular materials. Acta Mech. 164.